J. Fluid Mech. (1971), *vol.* 47, *part* 3, *pp.* 417–436
Printed in Great Britain

Structure of jets in rotating systems

By SULOCHANA GADGIL
Pierce Hall, Harvard University, Cambridge, Massachusetts†

(Received 21 July 1970)

An investigation of the structure of jets in rotating systems is presented. The fluid is assumed to be homogeneous and the flow laminar and quasi-geostrophic. When the rate of rotation is small, the dynamics is shown to be identical to that of jets in non-rotating systems, being a balance between inertial terms and lateral dissipation. As the rate of rotation increases the Ekman layers become important and in the strongly rotating case the friction in the Ekman layers dominates lateral dissipation. The jet in a non-rotating system entrains fluid at its edges and the downstream momentum flux is independent of the distance downstream. In the strongly rotating case, however, the jet ejects fluid at its edges and the downstream momentum flux decreases with downstream distance due to dissipation in the Ekman layers. A similarity solution for the general case with both types of friction is obtained and the transition from a jet in which lateral dissipation dominates to one in which Ekman friction is more important is discussed. General features of jets in strongly rotating systems are studied and implications for the Gulf Stream are mentioned.

1. Introduction

A jet can be defined as a flow in which the width or the cross-stream scale is much smaller than the downstream scale. Such flows occur along solid boundaries as in the case of wall jets or in the absence of solid boundaries as free jets. Free jets can be produced in the laboratory by means of an efflux from a narrow slit into a fluid placed in a container whose dimensions in the plane normal to the slit are large compared to the width of the slit, so that the fluid is essentially semi-infinite in the downstream and infinite in the cross-stream direction. The structure of free jets in non-rotating systems has been studied by Bickley (1937) and Schlichting (1933). The presence of free jets in the atmosphere and oceans like the Gulf Stream in the region east of Cape Hatteras, which remains coherent over distances which are much larger than its width, points to the importance of the investigation of free jets in rotating systems. In this paper the structure of free jets in homogeneous rotating fluids is studied with a view of gaining some understanding of this isolated feature of the general circulation. The framework used, however, is that of a laboratory experiment so as to ensure precise knowledge of all the parameters involved. The nature of the dissipation is also known because the experiments are assumed to be carried out in the laminar régime.

† Present address: Department of Meteorology, Massachusetts Institute of Technology, Cambridge, Massachusetts 02139.

2. Equations of the model

The model envisaged is that of a homogeneous fluid in a container with large horizontal dimensions and with a narrow vertical slit in one vertical wall through which the jet enters the container, placed on a rotating table with a vertical axis of rotation. The top and the bottom of the container are taken to be rigid and all the vertical walls with the exception of that containing the slit are taken to be porous so as to allow the jet to entrain or eject fluid without producing secondary circulations.

The origin of the co-ordinate system is taken to be the centre of the line of intersection of the slit and the horizontal bottom plane, the y axis is taken to be along this line and the x axis normal to it on the bottom plane and along the direction of flow of the incoming jet. The z axis is taken to be vertical and therefore coincident with the axis of rotation.

The pressure is assumed to be hydrostatic and only steady flows are considered. The equations for the conservation of momentum and mass are given in the usual notation as

$$uu_x + vu_y + wu_z - 2\Omega v = -(p_x/\rho_0) + \nu\nabla^2 u,$$

$$uv_x + vv_y + wv_z + 2\Omega u = -(p_y/\rho_0) + \nu\nabla^2 v,$$

$$p_z = 0,$$

$$u_x + v_y + w_z = 0.$$

Here Ω is the rate of rotation of the table and the pressure is that due to the relative motion of the fluid,

$$\frac{p}{\rho_0} = \frac{p_{\text{total}}}{\rho_0} + gz + \tfrac{1}{2}\Omega^2(x^2 + y^2).$$

The boundary conditions are of no slip and no normal flow at the top and bottom, viz

$$u = v = w = 0, \quad z = 0, H,$$

together with the conditions that the flow at the axis of the jet be along the axis and that the downstream velocity u and its derivatives u_y, u_{yy} vanish at large y:

$$v(y = 0) = 0,$$

$$u = u_y = u_{yy} = 0 \quad \text{at} \quad y = \pm\infty.$$

The equations are now non-dimensionalized. The scales in the y and z directions can be taken as the slit width Y_0 and the total height H of the container. There is no externally imposed downstream scale and hence x is scaled by X_0, which is unknown at this stage but will be determined as the scale of the dominant dissipation in § 3.1. The velocity field is scaled using the velocity at the slit along the axis $(U, UY_0/X_0, UH/X_0)$, so that no parameters appear in the equation of continuity. Non-dimensionalizing the pressure by the geostrophic scale $\rho_0 2\Omega UY_0$ the set of equations becomes

$$\epsilon[uu_x + vu_y + wu_z] - v = -p_x + (E/\delta)\, u_{zz} + (\sigma/\delta)\,(u_{yy} + \delta^2 u_{xx}), \qquad (2.1)$$

$$\delta^2\epsilon[uv_x+vv_y+wv_x]+u=-p_y+E\delta v_{zz}+\sigma\delta(v_{yy}+\delta^2 v_{xx}), \tag{2.2}$$

$$0=p_z, \tag{2.3}$$

$$u_x+v_y+w_z=0, \tag{2.4}$$

where

$$\epsilon=U/2\Omega Y_0, \quad E=\nu/2\Omega H^2, \quad \sigma=\nu/2\Omega Y_0^2, \quad \delta=Y_0/X_0. \tag{2.5}$$

The boundary conditions are

$$u=v=w=0, \quad z=0,1, \tag{2.6}$$

$$v(y=0)=0, \tag{2.7}$$

$$u=u_y=u_{yy}=0 \quad \text{at} \quad y=\pm\infty. \tag{2.8}$$

The flow is assumed to be quasi-geostrophic so that

$$\epsilon, \delta, \sigma/\delta, E^{\frac{1}{2}}/\delta \ll 1.$$

The flow will be in the form of a jet if δ is small.

The condition $E^{\frac{1}{2}}/\delta \ll 1$ together with the hydrostatic equation (2.3) implies that vertical shear will be confined to Ekman layers near the top and bottom. If the local Rossby number $u/2\Omega y \ll 1$, the conventional linear Ekman theory applies. Furthermore, it has been shown that jet-like solutions to the above set of equations can be obtained only if the scale X_0 is such that $\sigma/\delta \lesssim \epsilon$. Hence in the interior, away from the Ekman layers, the velocity and pressure field are expanded in powers of the Rossby number ϵ. We have, for example,

$$u=u_0+\epsilon u_1+\ldots.$$

The equations for the zeroth order are

$$v_0=p_{0x}, \tag{2.9}$$

$$u_0=-p_{0y}, \tag{2.10}$$

$$0=p_{0z}, \tag{2.11}$$

$$u_{0x}+v_{0y}+w_{0z}=0. \tag{2.12}$$

Combining equations (2.9), (2.10) and (2.12) with the condition (2.6) for the vertical velocity,

$$w_0=0.$$

The conditions of no normal flow at the top and bottom are satisfied by the interior solution. The Ekman layers are required to satisfy the conditions (2.6) on the horizontal components of the velocity. The equations for the Ekman layers are

$$v_0=p_{0x}-(E/\delta)\,u_{0zz},$$

$$u_0=-p_{0y}+E\delta v_{0zz}.$$

It can be shown that the magnitudes of the two components u_0 and v_0 become comparable in the Ekman layers giving

$$u_0^E=u_0+e^{-\zeta}[-u_0\cos\zeta-\delta v_0\sin\zeta],$$

$$v_0^E = v_0 + e^{-\zeta}[-v_0\cos\zeta + (u_0/\delta)\sin\zeta],$$

$$\zeta = z/(2E)^{\frac{1}{2}},\ 1-z/(2E)^{\frac{1}{2}} \quad \text{near} \quad z = 0, 1 \quad \text{respectively.}$$

The net effect of the Ekman layers on the interior flow is a vertical velocity at the edge produced by the divergence in the layer. This velocity can be obtained by integration of the equation of continuity across the layer (Robinson 1965, pp. 513–15) as

$$w(z = 1, 0) = \pm(1/\delta)(E/2)^{\frac{1}{2}}(u_{0y} - \delta^2 v_{0x}).$$

Since u and v are independent of z in the interior, (2.4) implies

$$w_{zz} = 0.$$

Hence

$$w = -(1/\delta)(E/2)^{\frac{1}{2}}(u_{0y} - \delta^2 v_{0x})(1-2z).$$

The vertical velocity produced by the Ekman layers is of order $(E^{\frac{1}{2}}/\delta)$ (i.e. $\ll 1$ and appears in the first-order equations, which are

$$u_0 u_{0x} + v_0 u_{0y} - v_1 = -p_{1x} + (\sigma/\epsilon\delta)u_{0yy} + O(\delta^2),$$

$$u_1 = -p_{1y} + O(\delta^2),$$

$$0 = p_{1z},$$

$$u_{1x} + v_{1y} + ((2E)^{\frac{1}{2}}/\delta\epsilon)u_{0y} = O(\delta^2).$$

The vorticity equation is

$$(u_0 u_{0x} + v_0 u_{0y})_y = (\sigma/\epsilon\delta)u_{0yyy} - ((2E)^{\frac{1}{2}}/\delta\epsilon)u_{0y}.$$

This can be integrated once to give

$$u_0 u_{0x} + v_0 u_{0y} = (\sigma/\delta\epsilon)u_{0yy} - ((2E)^{\frac{1}{2}}/\delta\epsilon)u_0. \tag{2.13}$$

The arbitrary function of x arising from the integration is seen to be zero on account of the boundary conditions (2.8). The basic equations of the jet are (2.9), (2.10) and (2.13). Since we will deal only with these equations in what follows, the subscript zero will be dropped.

3. Discussion of the governing equations

3.1. *Determination of the downstream scale*

Consider the vorticity equation (2.13) with the geostrophic equations (2.9) and (2.10):

$$uu_x + vu_y = -Ru + \alpha u_{yy}, \tag{3.1}$$

$$u = -p_y, \tag{3.2}$$

$$v = p_x, \tag{3.3}$$

where

$$R \equiv (2E)^{\frac{1}{2}}/\epsilon\delta = 2Y_0(\Omega\nu)^{\frac{1}{2}}/\delta UH, \tag{3.4}$$

$$\alpha \equiv \sigma/\epsilon\delta = \nu/\delta UY_0, \tag{3.5}$$

$$R/\alpha = (2E)^{\frac{1}{2}}/\sigma = [2Y_0^2/\nu](\Omega\nu/H^2)^{\frac{1}{2}} = Y_0^2/(\nu \times \text{spin-up time}). \tag{3.6}$$

There are two mechanisms of dissipation of vorticity on the right-hand side of (3.1). The first term arises from dissipation in the Ekman layers near the top and bottom and will be referred to as bottom friction in what follows. The second term represents lateral dissipation which will also be called side friction. The ratio of the two terms, R/α, is known in any experimental situation in terms of the rotation rate, slit width and the total height of the container (3.6) and is seen to increase with increasing rotation rate Ω. This ratio R/α is in fact the ratio of the time corresponding to the lateral diffusion over one slit width and the spin-up time and measures the relative efficiencies of the two mechanisms of dissipation. Each of these mechanisms gives a characteristic downstream scale which is the product of the velocity U and the characteristic dissipation time, the scale corresponding to the more efficient process being the shorter of the two. The downstream scale X_0 of the jet, therefore, has to be that corresponding to the dominant dissipation. In other words, the parameter δ is determined so as to make the dominant frictional term of the same order as the inertial terms.

If the rotation rate is slow so that $R \ll \alpha$ we have from (3.5)

$$\delta = \nu/UY_0 = 1/Re; \quad X_0 = UY_0^2/\nu. \tag{3.6a}$$

Thus in this case the downstream scale is given as the product of the slit width and the Reynolds number at the slit, Re. Note that the set of equations (3.1)–(3.3) reduce to those governing the structure of jets in non-rotating systems. The only effects of rotation, in this case, have been to make the flow two-dimensional (Taylor–Proudman theorem) and to produce a pressure field which is different from the non-rotating case.

On the other hand, if bottom friction dominates lateral friction we have, from (3.4),

$$\delta = 2Y_0(\Omega\nu)^{\frac{1}{2}}/UH; \quad X_0 = UH/2(\Omega\nu)^{\frac{1}{2}}. \tag{3.6b}$$

It is interesting that the downstream scale X_0 is in this case independent of the slit width.

If both side friction and bottom friction are comparable in magnitude all the terms in the vorticity equation are important and the two expressions for δ obtained above become equal and give the same downstream scale.

So far we have taken the cross-stream scale Y_0 to be the width of the slit. This was done so as to ensure the knowledge of the ratio R/α and hence the dynamics of the particular jet obtained in a given experiment. However, the width of the side-frictional jet is known to increase with distance downstream of the slit. Hence, if the ratio R/α were based upon the local width of the jet, it would increase with increasing x for this jet. The variation of the two dissipation mechanisms with distance from the slit can be studied by using in the cross-stream direction an internal scale $\overline{Y}$ defined by

$$R/\alpha = 1, \quad \text{i.e.} \quad \overline{Y} = \nu H/2(\Omega\nu)^{\frac{1}{2}}.$$

The ratio of the local width of the jet and the scale $\overline{Y}$ there determines whether bottom or side friction is dominant. Note that, for this choice of the cross-stream scale, the downstream scales (3.6*a*, *b*) coincide.

If the width of the slit is smaller than $\overline{Y}$, the dynamics near the slit is that of

a side frictional jet. As the distance from the slit increases, the local width increases, bottom friction becomes more important and finally dominates lateral dissipation at large distances from the slit. On the other hand, if the slit width is larger than $\overline{Y}$, bottom friction dominates side friction near the slit. If, in addition, the width of this bottom frictional jet increases with x, lateral dissipation becomes even less important as the distance from the slit increases. Thus, whereas bottom friction always dominates at sufficiently large distances from the slit, side friction is important near the slit only when the slit is narrower than $\overline{Y}$. In what follows, the statement R/α is small (large) is, therefore, equivalent to the statement that the point under consideration is at a sufficiently small (large) distance from a narrow slit. The transition from a Schlichting jet to a bottom frictional jet is discussed in § 5.1.

3.2. *Some general characteristics of jets in a rotating system*

Before obtaining solutions of the equations (3.1)–(3.3) for various values of the ratio R/α, it is worthwhile to consider some general properties of jet-like solutions of (3.1).

At the axis of the jet ($y = 0$) the cross-stream velocity v vanishes, (2.16). If $\alpha \neq 0$, then $u(x, y)$ has a proper maximum at $y = 0$,

$$u_y(y=0) = 0, \quad u_{yy}(y=0) < 0.$$

Hence for all R and α, from equation (3.1) at $y = 0$ we have

$$u_x(0) < 0. \tag{3.7}$$

Since $y = 0$ is a streamline and the pressure is the stream function, we can take

$$p(y = 0) = 0.$$

The total transport in the x direction is

$$T = \int_{-\infty}^{\infty} u\, dy = -\int_{-\infty}^{\infty} p_y\, dy = p(x, y = -\infty) - p(x, y = +\infty).$$

Here $p(y = \pm\infty)$ are the values of the pressure at the two edges of the jet. If the total transport T is in the positive x direction we must have

$$p(y = -\infty) > 0, \quad p(y = +\infty) < 0. \tag{3.8}$$

Note that (3.8) does not rule out counter-currents. To determine the nature of the solution near the two edges of the jet one can linearize about the pressure at the edges,

$$p = p(x) + p_1(x, y), \quad p_1 \ll p.$$

Substitution in (3.1)–(3.3) yields, upon neglecting the non-linear terms,

$$V p_{1yy} = \alpha p_{1yyy} - R p_{1y}.$$

Hence

$$u_1 \propto e^{ky},$$

where k at the two edges is given as

$$k = \frac{V(\pm\infty) + [V^2(\pm\infty) + 4R\alpha]^{\frac{1}{2}}}{2\alpha}; \quad \frac{V(\pm\infty) - [V^2(\pm\infty) + 4R\alpha]^{\frac{1}{2}}}{2\alpha}.$$

When side friction dominates bottom friction, there is only one root,

$$R \ll \alpha \sim 1, \quad k \approx V(\pm\infty)/\alpha.$$

Similarly, when bottom friction is dominant,

$$\alpha \ll R \sim 1, \quad k \approx -R/V(\pm\infty).$$

Thus the velocity u will decay exponentially at the two edges $y = \pm\infty$ only if

$$\left.\begin{aligned} R \ll \alpha \sim 1: &\quad V(\pm\infty) = \mp, \\ \alpha \ll R \sim 1: &\quad V(\pm\infty) = \pm. \end{aligned}\right\} \tag{3.9}$$

This implies that the bottom-frictional jet ejects fluid at both sides of the jet while the side-frictional jet entrains fluid at the edges. For the side-frictional jet, vorticity is conserved, but diffuses laterally. To counteract this diffusion, inflow is required. For the bottom-frictional jet, on the other hand, vorticity is decaying but not diffusing. To maintain it on the edges of the jet, outward advection is required. The total transport T increases in the former and decreases in the latter case, as can be seen from

$$\frac{\partial T}{\partial x} = \frac{\partial}{\partial x}\int_{-\infty}^{\infty} -p_y dy = V(-\infty) - V(+\infty).$$

If both lateral friction and bottom friction are equally important, exponentially decaying solutions exist for both ejecting and entraining jets.

The momentum across the jet at any given x is

$$J = \int_{-\infty}^{\infty} u^2 dy.$$

If a solution of (3.1)–(3.3) satisfies the boundary conditions for large y (2.8), it can be shown by integration of equation (3.1) that J satisfies

$$\partial J/\partial x = -R\int_{-\infty}^{\infty} u\, dy = -RT. \tag{3.10}$$

Thus if the rate of rotation is slow so that $R \ll \alpha$ the downstream momentum flux across the jet remains the same for all x, whereas for the cases $R \sim \alpha$, $R \gg \alpha$ the momentum is dissipated in the Ekman layers and decreases with downstream distance.

4. Similarity solutions

In this problem the downstream scale is not imposed externally. This suggests the existence of similarity solutions, i.e. solutions in which the scale of the velocity at the axis and the width of the jet depend only upon the distance from the slit. Assumption of a similar form reduces the two-dimensional problem (3.1)–(3.3) to one dimension and yields a solution which is independent of the details of the velocity profile at the inlet. The existence of a unique similarity solution suggests that an arbitrary velocity profile at the slit will go over into this similar profile at some distance downstream. For the case $R = 0$ which

corresponds to a jet in a non-rotating system, it has been shown experimentally by Sato & Sakao (1964) that the parabolic velocity profile at the slit changes over to the similar profile obtained by Schlichting within a distance less than five slit widths from the slit. Thus it seems reasonable to investigate similarity solutions of the equations (3.1)–(3.3) also for the cases $R/\alpha \gg 1$, $R \sim \alpha$.

4.1. *Schlichting's solution*

The similar profile for the side-frictional jet was obtained by Bickley (1937) and Schlichting (1933). We recapitulate briefly Schlichting's (1968, p. 744) treatment. Assuming a similar pressure distribution of the form

$$p = f(x)\,F(\eta), \quad \eta = yg(x), \tag{4.1}$$

equations (3.1)–(3.3) for the case $R = 0$ yield

$$(f'g + fg')\,F'^2 - gf'FF'' = -\alpha g^2 F'''. \tag{4.2}$$

The boundary conditions are

$$F(0) = F''(0) = 0, \quad F'(\pm\infty) = F''(\pm\infty) = 0. \tag{4.3}$$

If the functions $f(x)$ and $g(x)$ are chosen so that (4.2) for F has coefficients which depend only on η they are given as

$$f(x) = (a+bx)^l, \quad g(x) = (a+bx)^m, \tag{4.4}$$

$$l - m = 1. \tag{4.5}$$

The equation (4.2) thus provides only one relation between the exponents l and m. Any solution of (4.2) which satisfies the boundary conditions for large η (4.3) must satisfy the constraint on momentum flux J implied by (3.10) for the case $R = 0$,

$$(\partial/\partial x)\int_{-\infty}^{\infty} u^2\,dy = 0. \tag{4.6}$$

Substitution of (4.1) and (4.4) into (4.6) gives another relation between l and m thereby determining them,

$$2l + m = 0.$$

Hence

$$l = \tfrac{1}{3}, \quad m = -\tfrac{2}{3}. \tag{4.7}$$

The sign of the constant b is determined by using (3.7),

$$u_x(y=0) = \frac{b(l+m)}{a+bx}\,u(y=0) < 0.$$

Thus

$$b > 0.$$

Substitution of (4.1), (4.4) and (4.7) in (4.2) gives

$$F'^2 + FF'' = (3\alpha/b)\,F'''. \tag{4.8}$$

Integrating and choosing the constants so that the width and the velocity component along the axis at the slit are unity, we get

$$\left.\begin{aligned} p &= -(1+6\alpha x)^{\frac{1}{3}} \tanh\left[y(1+6\alpha x)^{-\frac{2}{3}}\right], \\ u &= (1+6\alpha x)^{-\frac{1}{3}} \operatorname{sech}^2\left[y(1+6\alpha x)^{-\frac{2}{3}}\right], \end{aligned}\right\} \tag{4.9}$$

$$\left.\begin{aligned} v(y = \pm\infty) &= \mp 2\alpha(1+6\alpha x)^{-\frac{2}{3}}, \\ T &= \int_{-\infty}^{\infty} u\,dy = 2(1+6\alpha x)^{\frac{1}{3}}. \end{aligned}\right\} \tag{4.10}$$

The velocity at the axis of the jet decreases with the downstream distance x and the transport increases with x due to entrainment of fluid at the edges of the jet as shown in § 3.2. The streamlines for this solution are shown in figure 1. The velocity profile, and the variation of the velocity at the axis and the width with x obtained by Sato & Sakao (1964), in an experiment of a jet in air, are shown in figure 2.

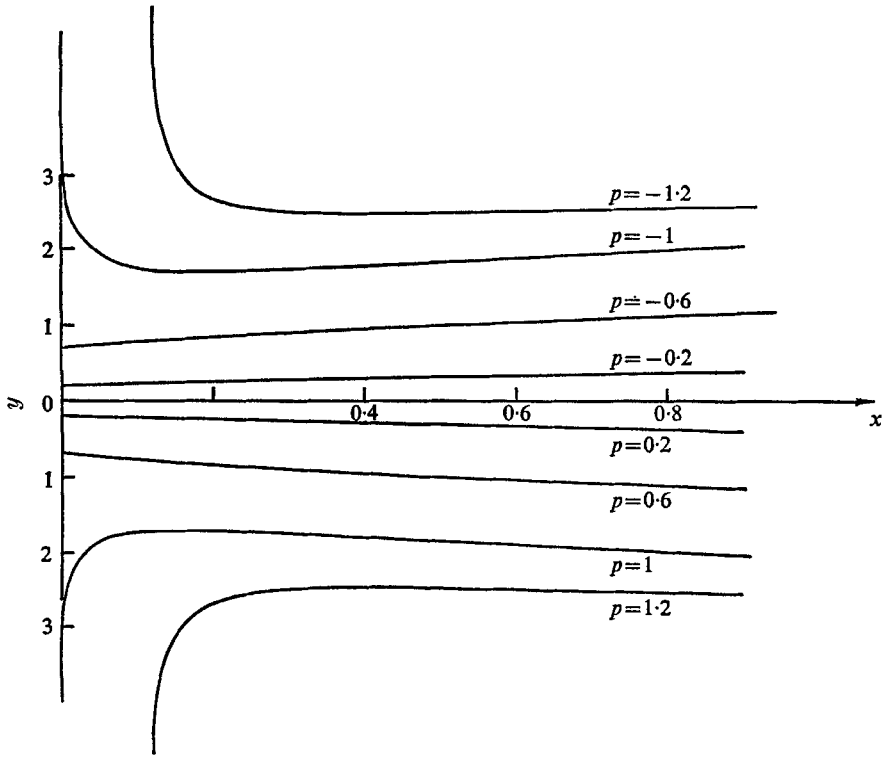

FIGURE 1. Streamlines for the side-frictional jet ($R = 0$).

4.2. *Bottom-frictional jet*

We investigate similarity solutions of equations (3.1) to (3.3) for the case $\alpha = 0$, i.e. when bottom friction is dominant. Substitution of the similar form (4.1) in the equations yields

$$(f'g+fg')F'^2 - gf'FF'' = RF', \tag{4.11}$$

with

$$F(0) = 0, \quad F'(\pm\infty) = 0.$$

As in the previous case, if $f(x)$ and $g(x)$ are chosen so that the equation for F has coefficients that depend only on η they have to be of the form (4.4) with one relation between the exponents l and m given as

$$l+m = 1. \tag{4.12}$$

The equation (3.10) cannot, however, be used in this case to determine l and m, because it is satisfied for all l and m satisfying (4.12). In order to restrict the allowable values of l, i.e. the values of l which will give acceptable solutions, we have to consider the other general properties of bottom-frictional jets discussed in § 3.2. The pressure in this case is given as

$$p(x,y) = (a+bx)^l F(y(a+bx)^{1-l}).$$

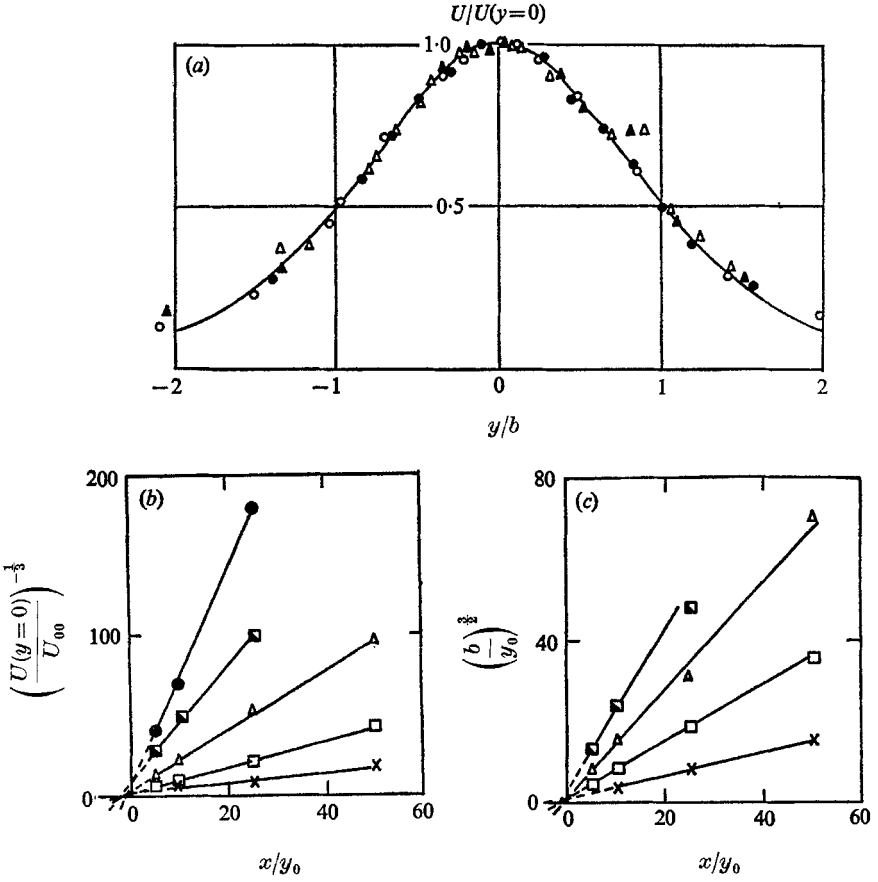

FIGURE 2. (*a*) Plot of $U/U(y=0)$ versus y/b, where b is the half-width, and the theoretical solution (4.9). ●, x = 1 mm; ○, x = 2 mm; ▲, x = 5 mm; △, x = 10 mm. (*b*) Downstream variation of central velocity. ●, U_{00} = 88 cm/s; ◪, U_{00} = 117 cm/s; △, U_{00} = 173 cm/s; □, U_{00} = 313 cm/s; ×, U_{00} = 770 cm/s. (*c*) Downstream variation of the half-breadth (after Sato & Sakao 1964).

Hence
$$u = -(a+bx)F'(\eta), \tag{4.13a}$$
$$v(\eta = \pm\infty) = bl(a+bx)^{l-1}F(\eta = \pm\infty), \tag{4.13b}$$
$$u_x(\eta = 0) = b/(a+bx)\,u(\eta = 0).$$

Using the conditions (3.7) at the axis, and the conditions (3.8) and (3.9) at large η, we get

$$b < 0; \quad l > 0.$$

The equation for F is

$$F'^2 - lFF'' = (R/b)\,F'. \tag{4.14}$$

Since $F'(0) = R/b$

$$u(\eta = 0) = (-(aR/b) - Rx).$$

We may set $b = -R$ without loss of generality. The equation (4.14) can be integrated once to yield, in terms of an arbitrary constant K,

$$F' = -1 + KF^{1/l}, \tag{4.15}$$

i.e. $$F'' = \frac{K}{l} F^{1/l-1} F'; \quad F''' = \frac{K}{l}\left(\frac{1}{l} - 1\right) F^{1/l-2} F'^2 + \frac{K}{l} F^{1/l-1} F''.$$

In general

$$\frac{\partial^{k+1} F}{\partial \eta^{k+1}} = \frac{K}{l}\left(\frac{1}{l} - 1\right) \ldots \left(\frac{1}{l} - k\right) F^{1/l-k-1} F'^{k+1} + \ldots.$$

If we demand that F'' and all higher derivatives of F remain finite at the axis where F vanishes, l has to be the reciprocal of an integer. Also, it is evident from the equation (4.15) that F'', F''' and higher derivatives vanish with F' which must occur at the two edges of the jet. The values of F at these points at which F', F'', etc. vanish are proportional to the asymptotic pressure at the two edges and are given as

$$F^{1/l} = 1/K. \tag{4.16}$$

For the downstream velocity to vanish at both edges of the jet, the equation (4.16) must have at least two roots, the difference between the roots being the total transport in the x direction. This implies that $1/l$ has to be an even number. If the constant K is chosen so that the total transport on each side of the jet is unity at the slit, the acceptable solutions of the bottom-frictional jet are

$$F' = -1 + F^{2n}. \tag{4.17}$$

These are illustrated in figure 3 for various values of n. The area under each curve is the momentum J for a fixed transport at a given x and is seen to decrease as n increases. Thus, we have a whole set of acceptable similarity solutions for the bottom-frictional jet. Further analysis will identify one amongst this set as the solution which will be obtained in an experiment.

It is interesting to note in passing that Rossby's (1951) conjecture that the profile of a jet should be that corresponding to the minimum momentum for a given transport, based on the observation that jets occur in the atmosphere wherever momentum losses are incurred through friction, would suggest that the profile with $n = 1$ is the 'correct' profile.

4.3. *Similarity solution for the general case*

When both side friction and bottom friction are important, substitution of th similar pressure distribution (4.1) gives the equation governing F,

$$(f'g + fg')\,F'^2 - f'gFF'' = RF' - \alpha g^2 F'''. \tag{4.18}$$

Again choosing $f(x)$ and $g(x)$ so that the equation for F contains no functions of x we get (4.4) and two relations between the exponents l and m,

$$l + m = 1, \quad l - m = 1.$$

Hence

$$l = 1, \quad m = 0, \tag{4.19}$$

$$p = (a - bx)\,F(y), \quad b > 0. \tag{4.20}$$

In this case l and m are completely determined by (4.18) because of the extra term appearing on the right-hand side. The similar form is seen to be rather special in that the x and y dependence is separable. The equation and the boundary conditions for F are

$$F'^2 - FF'' = -(R/b)\,F' + (\alpha/b)\,F''', \tag{4.21}$$

$$F(0) = F''(0) = 0, \tag{4.22}$$

$$F'(\pm\infty) = F''(\pm\infty) = 0. \tag{4.23}$$

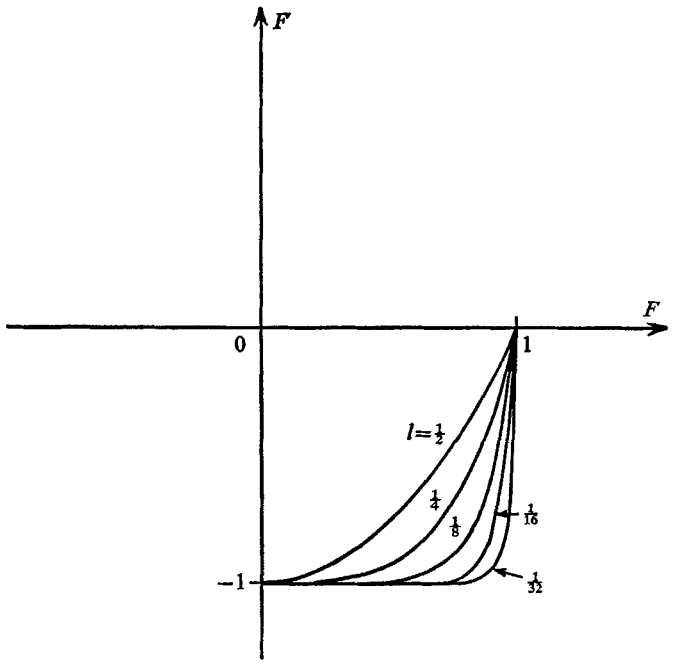

FIGURE 3. Phase plane representation of the similarity solutions for the bottom-frictional case ($\alpha = 0$). Plot of $F'(= -U)$ versus F for $F' = -1 + F^{1/l}$.

Note that (4.21) does not reduce to (4.8) for the side-frictional jet in the limit of vanishing R. Since it was shown in § 4.2 that the solutions of the form (4.4) for the case $R = 0$ can satisfy the boundary conditions only if the exponents l and m satisfy (4.7), it is clear that solutions of (4.21) with $R = 0$ will not satisfy the boundary conditions. Thus we do not expect any jetlike solutions of (4.21) to (4.23) for small R.

Solutions of (4.21) with R and α of comparable magnitude cannot be obtained analytically. Numerical investigation is facilitated by conversion of the problem with boundary conditions (4.22) and (4.23) at $y = 0$ and ∞ to one with all boundary conditions at $y = 0$. The unknown condition $F'(0)$ is then varied and the behaviour of the solution observed in the search for a solution which satisfies the condition (4.23) at infinity. This was done with the help of an analog computer for (4.8) for Schlichting's jet and for (4.21). In the former case a unique

solution satisfying the boundary conditions for large η was obtained but the search in the latter case showed that no solutions satisfying the boundary conditions existed. The unique solution obtained for the former case implies that it is highly improbable that the non-existence of solutions in the latter case was due to computational errors.

The remaining case $R \gg \alpha$ was then investigated. The equation (4.21) for the case $\alpha = 0$ yields a solution of the form

$$\left.\begin{aligned} F &= \mp 1 \pm e^{\mp y} \\ F' &= -e^{-|y|} \end{aligned}\right\} \quad (y \gtrless 0). \tag{4.24}$$

This solution has a discontinuity in $F''(0)$, i.e. in u_y corresponding to a cusp in the velocity profile, which has to be removed by lateral dissipation. The boundary-layer nature of (4.21) for small α suggests the possibility of a boundary layer near the axis capable of removing the cusp. Substitution of the boundary-layer velocity of the form

$$F' = -1 + \alpha^c G(y/\alpha^c),$$

which is chosen so as to ensure that F'' is the same order in the boundary layer and the exterior, yields

$$c = \tfrac{1}{2}, \quad \xi = y/\alpha^{\frac{1}{2}};$$

$$GG_{\xi\xi} = G_\xi G_{\xi\xi\xi} - G_{\xi\xi}^2 + O(\alpha^{\frac{1}{2}}).$$

This equation can be integrated to give

$$F'' = G_\xi = D\int_0^\xi e^{\frac{1}{2}\xi^2}\,d\xi = (D/\alpha^{\frac{1}{2}})\int_0^y e^{y^2/2\alpha}\,dy.$$

This solution is clearly unacceptable. Thus the discontinuity in F'' cannot be removed by a boundary layer near the axis and we may conclude that there are no solutions of the form (4.20) for the general case $R \neq 0$, $\alpha \neq 0$ which satisfy the boundary conditions for large y. We may emphasize that (4.21) implied by the form (4.20) does not reduce to that governing the unique similarity solution for the side-frictional case.

5. Solution for the general case and the resolution of the non-uniqueness of similar solutions for the bottom-frictional jet

The analysis so far has shown that, when the particular similarity form (4.1) and (4.4) is assumed, there is a unique solution for the side-frictional jet and a set of solutions for the bottom-frictional jet. The discussion at the end of § 3.1 showed that, if the ratio R/α is based upon the local width, it increases with downstream distance for a Schlichting jet, implying thereby a transition of the Schlichting jet to a bottom-frictional jet at some distance from the slit. This suggests that the solution for the general case $R \neq 0$, $\alpha \neq 0$ will be a continuous function of the parameters R and α which reduces to the known Schlichting solution at $R = 0$, and yields one of the set of solutions (4.15) for the bottom frictional jet in the limit of vanishing α. In this section, such a solution is found

by applying the von Mises transformation (Goldstein 1960, § 9.3) in which the pressure p is used as one of the independent variables. Substitution of

$$p_y = H(p, x)$$

in the equations (3.1)–(3.3) gives

$$H_x = R - \alpha(H_p^2 + HH_{pp}). \tag{5.1}$$

All the similarity solutions for the bottom-frictional jet (4.15) can be expressed in these co-ordinates as

$$H = -(1 - Rx) + p^{1/l}. \tag{5.2}$$

Schlichting's solution for the side-frictional jet is

$$H = -(1 + 6\alpha x)^{-\frac{1}{3}} + p^2/(1 + 6\alpha x). \tag{5.3}$$

This suggests looking for a solution of (5.1) of the form

$$H = -\phi(x) + \psi(x)\, p^j. \tag{5.4}$$

Substitution of (5.4) into (5.1) shows that non-trivial solutions for $\phi(x)$ and $\psi(x)$ exist only for the case $j = 2$. For this case, the equation (5.4) can be integrated to give

$$p = -(\phi(x)/\psi(x))^{\frac{1}{2}} \tanh\,[y(\phi(x)\,\psi(x))^{\frac{1}{2}}], \tag{5.5}$$

$$u = \phi(x)\,\mathrm{sech}^2\,[y(\phi(x)\,\psi(x))^{\frac{1}{2}}].$$

Combining (5.1) and (5.4) with $j = 2$,

$$-\phi' + \psi' p^2 = R - \alpha[6\psi^2 p^2 - 2\phi\psi].$$

Since $\phi(x)$ and $\psi(x)$ do not depend on p,

$$\phi' = -R - 2\alpha\phi\psi, \quad \psi' = -6\alpha\psi^2. \tag{5.6}$$

If the arbitrary constants involved in the integration of (5.6) are chosen so that $u(0, 0)$ and the width of the jet at the slit are unity, the solutions in the three cases are given as

$$R = 0: \quad p = -(1 + 6\alpha x)^{\frac{1}{3}} \tanh\,[y(1 + 6\alpha x)^{-\frac{2}{3}}]; \tag{5.7}$$

$$\alpha = 0: \quad p = -(1 - Rx)^{\frac{1}{2}} \tanh\,[y(1 - Rx)^{\frac{1}{2}}], \tag{5.8}$$

$$u = (1 - Rx)\,\mathrm{sech}^2\,(y(1 - Rx)^{\frac{1}{2}}); \tag{5.9}$$

$$R \neq 0,\ \alpha \neq 0: \quad p = -\left[(1 + 6\alpha x)^{\frac{2}{3}}\left(1 + \frac{R}{8\alpha}\right) - \frac{R}{8\alpha}(1 + 6\alpha x)^2\right]^{\frac{1}{2}} \times \tanh\left[y\left(\frac{1 + R/8\alpha}{(1 + 6\alpha x)^{\frac{1}{3}}} - \frac{R}{8\alpha}\right)^{\frac{1}{2}}\right]. \tag{5.10}$$

This solution is of the similarity form (4.1) for all the cases. Note that the scale and width factors are not simple polynomials of the form (4.4) for the general case $R \neq 0$, $\alpha \neq 0$. The conventional method of choosing the functions $f(x)$ and $g(x)$ so as to ensure that the equation governing $F(\eta)$ has coefficients which depend only on η, forces them to be of the form (4.4) and hence does not reveal the solution (4.10). In this case the separation of variables is made possible by the simple form of $F(\eta)$ despite the complexity of $f(x)$ and $g(x)$.

It can be seen that the solution for the general case reduces to that of the side-frictional jet in the limit of vanishing R. The solution in the limit of small α

is the similarity solution for the case $n = 1$ in (4.17) and is, in fact, the profile which has minimum momentum for a given transport.

The cross-stream velocity at the two edges of the jet in the three cases is given as

$$\alpha = 0: \quad V(\pm\infty) = \pm R/2(1-Rx)^{\frac{1}{2}};$$

$$R = 0: \quad V(\pm\infty) = \mp 2\alpha/(1+6\alpha x)^{\frac{2}{3}};$$

$$R \neq 0, \alpha \neq 0: \quad V(\pm\infty) = \mp \frac{(\frac{1}{2}R+4\alpha)(1+6\alpha x)^{-\frac{1}{3}} \pm \frac{3}{2}R(1+6\alpha x)}{2[(1+(R/8\alpha))(1+6\alpha x)^{\frac{2}{3}} - (R/8\alpha)(1+6\alpha x)^2]^{\frac{1}{2}}}.$$

The jet entrains fluid at its edges from the slit ($x = 0$) up to a distance x given by

$$(1+6\alpha x)^{\frac{4}{3}} = \tfrac{1}{3}(1+(8\alpha/R)).$$

In this region the transport increases with downstream distance. Note that this region extends over the entire length of the jet in the limit of vanishing R. For $R \neq 0$, the jet ejects fluid beyond this point, implying a downstream decrease in transport. The transition between the two régimes is smooth and all the features in the region of transition are intermediate between those of the side- and bottom-frictional jets. The velocity at the axis of the jet decreases with x and vanishes at a point given by

$$(1+6\alpha x)^{\frac{4}{3}} = 1+(8\alpha/R).$$

At this point, the cross-stream velocity equals Ry for finite y and becomes indeterminate as y tends to infinity. These features are characteristic of the bottom-frictional jets and can therefore be studied simply by considering the case $\alpha = 0$.

For the bottom-frictional jet, the velocity at the axis of the jet decreases with x and vanishes at the point $x = 1/R$. In dimensional terms this occurs at a distance of $UH/2(\Omega\nu)^{\frac{1}{2}}$ from the slit. The momentum flux in the x direction in this case is given by integration of (3.10) as

$$J = \tfrac{4}{3}(1-Rx)^{\frac{3}{2}}.$$

Thus the jet cannot penetrate beyond the point $x = 1/R$, because all the momentum has been dissipated in the Ekman layers. This is a general property of the bottom-frictional jet and holds for the whole class of similarity solutions, as can be seen from (4.13*b*). The cross-stream velocity at the point $x = 1/R$ is again Ry for finite y and becomes indeterminate for infinite y. This feature is common to all similarity solutions of this class with the exception of the case $l = 1$ as shown in (4.13*b*). Note that the final demise of the jet at $x = 1/R$ cannot be discussed in terms of this model because our assumption $\delta \ll 1$ is violated in the vicinity of this point. The behaviour of our solution in this region should therefore be considered merely as an indication of a trend. The streamlines for the bottom-frictional jet (5.7) are shown in figure 4. They may be compared to those of an entraining jet shown in figure 1. The velocity profile is the same in both cases.

The vanishing of the downstream velocity u at the point $x = 1/R$ and the behaviour of the cross-stream velocity v at this point are two features of the strongly rotating case $\alpha = 0$. In order to see if these would occur in an experiment, an initial-value problem in x is done in the next section.

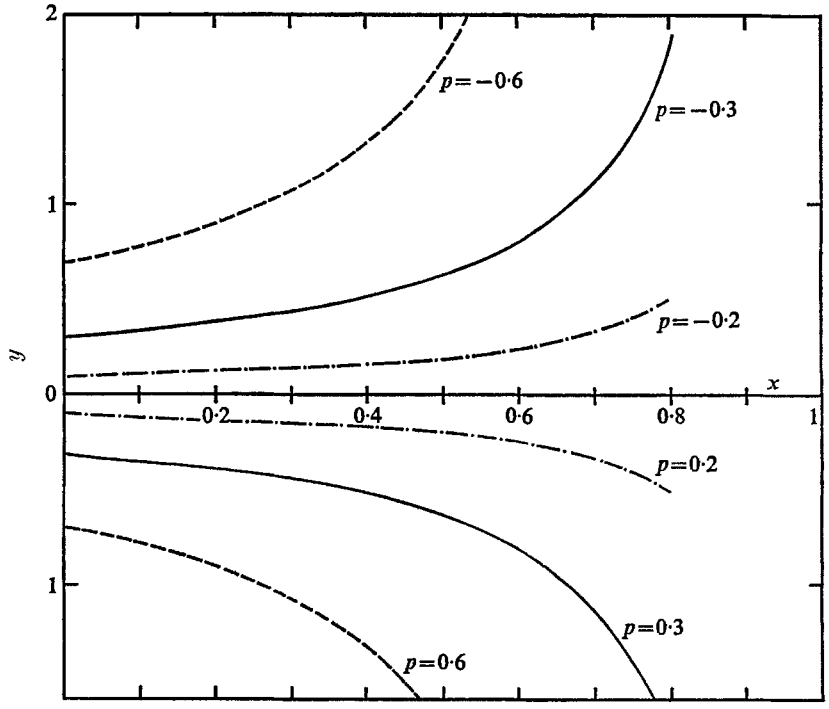

FIGURE 4. Streamlines for the bottom-frictional jet, $\alpha = 0$.

6. Initial-value problem for the bottom-frictional jet

The equation (5.1) is a first-order equation in the downstream distance x. Thus, given the velocity and pressure at any x, and in particular $x = 0$, this can be integrated to yield a solution for those particular inlet conditions. This has been done for two inlet conditions. For the case $\alpha = 0$, (5.1) can be integrated to give

$$H = Rx + h(p). \tag{6.1}$$

For

$$\left.\begin{aligned} p(0,y) &= -\tanh y, \\ p_y(0,y) &= -\operatorname{sech}^2 y = p^2 - 1, \\ h(p) &= H(p,0) = p^2 - 1. \end{aligned}\right\} \tag{6.2}$$

Upon substitution of (6.2), equation (6.1) can be integrated to give

$$p = -(1-Rx)^{\frac{1}{2}} \tanh\left(y(1-Rx)^{\frac{1}{2}}\right),$$

$$u = (1-Rx)\operatorname{sech}^2\left(y(1-Rx)^{\frac{1}{2}}\right).$$

This is identical to the similarity solution (5.8) and (5.9) for the bottom-frictional jet. Thus if the velocity profile is of a similar form at any x, it remains unchanged with distance downstream, as is expected. In an experiment, the profile at the slit is not, in general, a similar profile. In order to see how a general profile changes with x, consider

$$p(0,y) = -\tan^{-1} y,$$

$$p_y(0,y) = -1/(1+y^2) = -\cos^2 p,$$

$$h(p) = H(p,0) = -\cos^2 p.$$

Substitution into (6.1) and integration yields

$$p = -\tan^{-1}[\{(1-Rx)/Rx\}^{\frac{1}{2}}\tanh(y\{Rx(1-Rx)\}^{\frac{1}{2}})], \tag{6.3a}$$

$$u = -p_y = \frac{Rx(1-Rx)\operatorname{sech}^2(y\{Rx(1-Rx)\}^{\frac{1}{2}})}{1-(1-Rx)\operatorname{sech}^2(y\{Rx(1-Rx)\}^{\frac{1}{2}})}, \tag{6.3b}$$

$$v = \frac{[R/\{Rx(1-Rx)\}^{\frac{1}{2}}]\tanh(y\{Rx(1-Rx)\}^{\frac{1}{2}}) + Ry(2Rx-1)\operatorname{sech}^2(y\{Rx(1-Rx)\}^{\frac{1}{2}})}{2[1-(1-Rx)\operatorname{sech}^2(y\{Rx(1-Rx)\}^{\frac{1}{2}})]}. \tag{6.3c}$$

It can be seen from (6.3*b*, *c*)

$$u(x=1/R) = 0,$$

$$v(y=\pm\infty) = \pm R/2\{Rx(1-Rx)\}^{\frac{1}{2}}.$$

Note that the above formula for v at $y = \pm\infty$ does not hold at $x = 0$ or $1/R$.

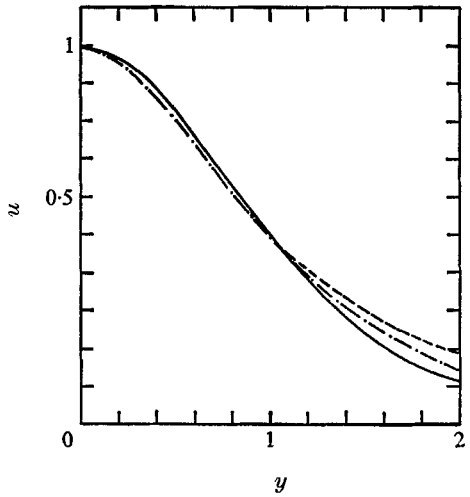

FIGURE 5. Plot of $U/U(y=0)$ versus y/L for the profile with $1/(1+y^2)$ as inlet condition at $x = 0{\cdot}1$ (– – –) and $x = 0{\cdot}4$ (–·–·–) together with the $\operatorname{sech}^2 y$ profile.

Thus the two features of the bottom-frictional jet at the point of its demise are inherent in the physics and not artifacts due to the assumption of similar profiles. It is of interest to note that the profile (6.3*b*) becomes more and more like the similar profile (5.9) as the distance x increases. This is shown in figure 5. To see if the initial trend of the parabolic profile is also towards the similar profile, the gradient $u_x(x = 0)$ has been plotted against y in figure 7, for the three profiles $1-y^2$, $\operatorname{sech}^2 y$ and $1/(1+y^2)$ which are shown in figure 6. Figure 7 indicates that initially both the profiles will tend towards the similar profile. It must be emphasized that this is only a plausibility argument and an experiment will have to be performed in order to test the results derived so far. In designing the experiment, in addition to the constraints on E, σ, ϵ, δ, the condition that the Reynolds number at the slit is small enough to ensure laminar flow has to be satisfied. Possible configurations for the two cases $R \gg \alpha$, $\alpha \ll R$ have been derived.

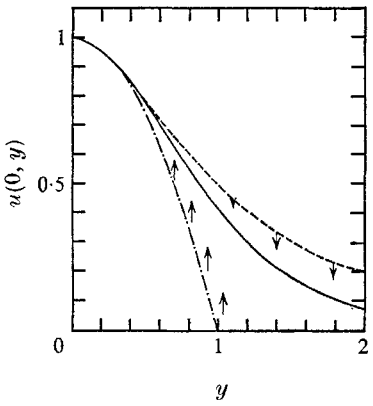

FIGURE 6

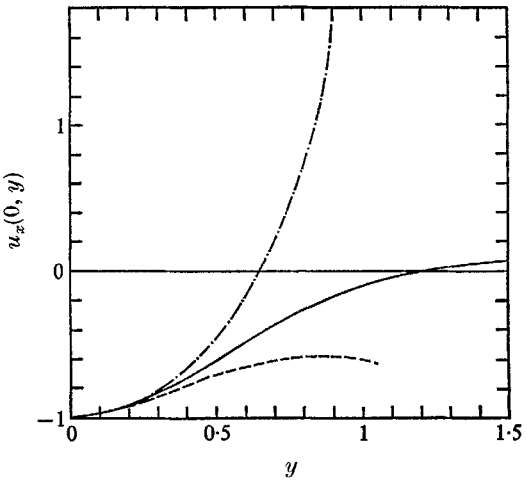

FIGURE 7

FIGURE 6. Plot of three profiles $1/(1+y^2)$ (– – –), $\mathrm{sech}^2 y$ and $1-y^2$ (–·–·–) against y. Arrows indicate the direction in which the profile will change.

FIGURE 7. Plot of $u_x(x=0)$ versus y for the three profiles of figure 6.

7. Implications for the Gulf Stream

In the region east of Cape Hatteras, the Gulf Stream can be considered as a free jet which extends to the bottom of the ocean and remains coherent over distances which are much longer than its width (Fuglister 1963). If the problem of determining the structure of the stream is considered to be separable from that of determining its meandering path, some understanding about the nature of the stream can be gained from the present investigation. Some justification for a model in which the variation of the Coriolis parameter with latitude (β effect) is neglected, lies in the fact that the mean path of the stream in this region makes a small angle with the east. The major drawback of this model is then the neglect of baroclinicity.

The frictional parameters for the stream can be estimated by using a quasi-laminar model with lateral eddy viscosity ν_H occurring in the parameter σ and a vertical eddy viscosity ν_V appearing in the Ekman number E. Webster's (1965) measurements of the velocity of the stream near Cape Hatteras yield a value of about $10^6\,\mathrm{cm^2\,sec^{-1}}$ for the magnitude of ν_H. In estimation of ν_V, we note that, since the upper surface of the stream is free, the no-slip condition is relevant only for the bottom and there is no Ekman layer near the top. Hence the eddy viscosity ν_V is that of the frictional layer underneath the stream and the coefficient of bottom friction in the vorticity equation (3.1) is now $\frac{1}{2}R$. Munk, Snodgrass & Wimbush (1970) have measured the velocity profile of the tidal currents near the bottom of the Pacific. Their observations indicate a turbulent Ekman layer, about 8 m in depth. This depth implies an equivalent eddy viscosity of $32\,\mathrm{cm^2\,sec^{-1}}$. We use this value of ν_V in estimation of the bottom friction for the Gulf Stream, the reason being that first there are no measurements of the benthic

Ekman layer of the Gulf Stream and secondly the velocity of the tidal currents above the benthic Ekman layer (5 cm/sec) is comparable with the observed bottom velocities of 10 cm/sec for the Gulf Stream (Fuglister 1963). Also, since our analysis is restricted to homogeneous jets, the velocity scale U is taken to be the computed depth average of the maximum velocity at each level from Fuglister's (1963) observations, i.e. 30 cm/sec. Using, in addition,

$$Y_0 = 100\,\text{km}, \quad H = 4\,\text{km}, \quad 2\Omega = 10^{-4}\,\text{sec}^{-1},$$

we get $$\epsilon = 0{\cdot}03, \quad \sigma = 10^{-4}, \quad (E/2)^{\frac{1}{2}} \approx 10^{-3}, \quad R/\alpha \approx 10.$$

It can be seen that all the assumptions of our model are satisfied by these parameters. Bottom friction dominates lateral dissipation for the particular ν_H and ν_V chosen. This is rather gratifying since the relevance of models with dominant lateral dissipation for the Gulf Stream is highly questionable in light of Webster's (1965) measurements of negative ν_H. If the stream is in fact a bottom-frictional jet, the downstream scale is

$$\epsilon Y_0 (2/E)^{\frac{1}{2}} = 3000\,\text{km}.$$

Fuglister (1963) interpreted the surface data as a narrow current extending for more than 2500 km which compares well with the downstream scale obtained. In addition, one would expect the velocity at the edges of the stream to correspond to ejection of fluid and the downstream momentum flux and the transport to decrease with downstream distance. These predictions are based upon the general characteristics of bottom-frictional jets.

It should be pointed out that there is one major difference between the flow in the experimental basin and an ocean circulation in which jets such as the Gulf Stream occur. In the former, the entire flow field is produced by the jet itself, whereas in the latter, the fluid away from the jet is driven by other forces such as wind. Our method of resolving the non-uniqueness of the similarity solutions for the bottom-frictional jet by demanding continuity in the parameters R and α may be correct for the former situation, but, in the latter, the velocity profile would be partially determined by the imposed asymptotic flow. The situation would then be intermediate between the experimental free jet and the classical flat plate boundary layer which is completely determined by the velocity field away from the plate. Thus, for jets occurring in an oceanic circulation, the position of the axis as well as the velocity profile depend upon the driving force and a complete understanding of the structure requires the solution of the whole circulation problem. This suggests the manner in which the β-effect, which is crucial in determination of the circulation in regions which are away from the boundary layers and jets, can influence the structure of the jet by determining the asymptotic flow at the edges of the jet. For example, it can be shown that, when the imposed asymptotic velocity is the Sverdrup velocity (Sverdrup 1947, equation (13)) produced by a zonal wind stress whose curl is negative in the southern part of the basin and positive in the northern part, the jet occurs along the line of zero wind-stress curl. The velocity profile is given by (4.20), (4.24) and its width is independent of downstream distance. The above result about position of the jet is consistent with the results of numerical experiments of Bryan

(1963) and Veronis (1966). The available wind-stress data is too sparse to allow a meaningful comparison fo the mean path of the Gulf Stream and the curve of zero wind-stress curl but they appear to be similar in shape and location.

I had stimulating discussions on the work presented with Professors D. J. Baker, N. P. Fofonoff, P. H. Stone and Dr J. R. Luyten. Professors F. P. Bretherton, G. F. Carrier and A. R. Robinson read the manuscript and made valuable suggestions. This research was supported by the Office of Naval Research under Contract NO014–67–A-0298–0011 to Harvard University.

REFERENCES

Bickley, W. 1937 The plane jet. *Phil. Mag.* (7) **23**, 727–731.

Bryan, K. 1963 A numerical investigation of a non-linear model of a wind-driven ocean. *J. Atmos. Sci.* **20**, 594–606.

Fuglister, F. C. 1963 Gulf Stream '60. In *Progress in Oceanography*, **1**, 265–373.

Goldstein, S. 1960 *Lectures on Fluid Mechanics*. Interscience.

Munk, W., Snodgrass, F. & Wimbush, M. 1970 Off-shore tides – transition from California coastal to deep sea waters. *Geophys. Fluid Dynam.* **1**, 161–236.

Robinson, A. R. 1965 Oceanography. In *Res. Frontiers in Fluid Dynamics* (ed. R. J. Seeger and G. Temple), pp. 504–533.

Rossby, C.-G. 1951 On the vertical and horizontal concentration of momentum in air and ocean currents, I. *Tellus*, **3**, 15–28.

Sato, H. & Sakao, F. 1964 An experimental investigation of the instability of two-dimensional jets at low Reynolds numbers. *J. Fluid Mech.* **20**, 337–352.

Schlichting, H. 1933 Laminare Strahlenausbreitung. *ZAMM* **13**, 260–263.

Schlichting, H. 1968 *Boundary Layer Theory*. McGraw Hill.

Sverdrup, H. U. 1947 Wind-driven currents in a baroclinic ocean: with application to the equatorial currents of the eastern Pacific. *Proc. Natn. Acad. Sci.* **33**, 318–326.

Veronis, G. 1966 Wind-driven ocean circulation. Part 2. *Deep-Sea Res.* **13**, 31–55.

Webster, T. F. 1965 Measurements of eddy fluxes of momentum in the surface layer of the Gulf Stream. *Tellus*, **17**, 239–245.